

## Article

# FeCo<sub>2</sub>S<sub>4</sub>/Ni foam: A Bimetallic Sulfide Electrocatalyst with Efficient and Robust Behavior

Jiayou Tao <sup>1</sup>, Shuhua Liu <sup>2</sup>, Yanmo Liao <sup>1,2</sup>, Hui Qiao <sup>2</sup>, Yu Liu <sup>1</sup>, Hui Chen <sup>1</sup>, Min Teng <sup>1</sup>, Yong Wei <sup>1</sup>, Sanjie Liu <sup>1</sup>, Zongyi Qiu <sup>3</sup>, Chang Li <sup>1,\*</sup> and Xiang Qi <sup>2,\*</sup>

<sup>1</sup> Key Laboratory of Hunan Province on Information Photonics and Freespace Optical Communications, School of Physics and Electrical Sciences, Hunan Institute of Science and Technology, Yueyang 414006, China

<sup>2</sup> School of Physics and Optoelectronics, Xiangtan University, Xiangtan 411105, China

<sup>3</sup> ZhongKe (Guangdong) Refinery & Petrochemical Company Limited, Zhanjiang 524076, China; qiuzongyi@163.com

\* Correspondence: lichang1226@163.com (C.L.); xqi@xtu.edu.cn (X.Q.)

**Abstract:** The development of effective, feasible, stable, and inexpensive electrocatalysts has been a great challenge in the field of overall water splitting (WS). Herein, a bifunctional electrocatalyst (BF ECS), FeCo<sub>2</sub>S<sub>4</sub> nanowire (FCS NWs/Ni)/nickel (Ni) foam, with superior HER/OER activity and stability was designed and fabricated using a hydrothermal method. In addition, this efficient method can be used for the synthesis of other bimetallic MCo<sub>2</sub>S<sub>4</sub> sulfides (M = Cu, Zn, Mn, etc.). Electrochemical experiments showed the as-synthesized FCS NWs/Ni exhibited overpotentials of 350.5, 203.7, 115.97, and 62.6 mV (0.05, 0.1, 0.2, and 1 M KOH) at the current density of  $-10 \text{ mA cm}^{-2}$  for HER, including small overpotentials of 1.51, 1.36, 1.24, and 1.11 V ( $10 \text{ mA cm}^{-2}$ ) in a 0.05, 0.1, 0.2, and 1 M KOH solution for OER. The FCS NWs/Ni has a splendid electrocatalytic performance which is related to the synergistic effect of cobalt, iron, and sulfur. Specifically, it has excellent electrical conductivity, a higher specific capacity, and a rich redox state of iron, cobalt, and sulfur elements. The results demonstrate a promising method for the design and fabrication of metal BF ECS for overall water splitting.

**Keywords:** FeCo<sub>2</sub>S<sub>4</sub>; OER; HER; bifunctional electrocatalyst



**Citation:** Tao, J.; Liu, S.; Liao, Y.; Qiao, H.; Liu, Y.; Chen, H.; Teng, M.; Wei, Y.; Liu, S.; Qiu, Z.; et al. FeCo<sub>2</sub>S<sub>4</sub>/Ni foam: A Bimetallic Sulfide Electrocatalyst with Efficient and Robust Behavior. *Crystals* **2023**, *13*, 717. <https://doi.org/10.3390/cryst13050717>

Academic Editor: Nabeen K Shrestha

Received: 13 March 2023

Revised: 17 April 2023

Accepted: 18 April 2023

Published: 24 April 2023



**Copyright:** © 2023 by the authors. Licensee MDPI, Basel, Switzerland. This article is an open access article distributed under the terms and conditions of the Creative Commons Attribution (CC BY) license (<https://creativecommons.org/licenses/by/4.0/>).

## 1. Introduction

Bifunctional (BF) electrocatalysts (ECS) for the oxygen evolution reaction (OER) and hydrogen evolution reaction (HER) have good application prospects in the field of energy storage [1,2]. In recent years, platinum-based, iridium-based, and ruthenium-based electrocatalysts have been considered the best choice for high-performance HER and OER electrocatalysts [3]. However, the wide application of precious metals as electrocatalysts is limited by the high cost and scarcity of resources. In addition, the HER catalyst reacts slowly in an alkaline solution and the OER catalyst reacts slowly in an acidic solution [4]. Considering the low-cost effect, the HER and OER of the working electrode catalyst should react at the same pH as the integrated electrolytic solutions [5]. Therefore, abundant attempts have been made to develop bifunctional electrocatalysts which can effectively catalyze the water splitting of HER and OER [6]. For instance, transition metal compounds (Fe [7], Co [8], Ni [9], and Mn [10]) have been widely researched both theoretically and experimentally. Regrettably, the development and application of these materials are hindered by their inherently low ECS performance.

Currently, broad ranges of non-precious metal ECS based on transition metal oxides (M<sub>x</sub>O<sub>y</sub>) [11] and double metal oxides (AB<sub>2</sub>O<sub>4</sub>) have gained attention due to their high ECT activity [12,13]. Li et al. [14] reported that the MnFe<sub>2</sub>O<sub>4</sub>/Fe hybrid nanoparticles possess superior ECT performance in alkaline media. Furthermore, Jin et al. [15] reported that the BF ECT activities of metal oxides are mainly determined by the  $\sigma^*$ -orbital ( $e_g$ )

occupation of metal cations in the octahedral centers. Among several cobalt oxides [16], the surface  $\text{Co}^{3+}$  are referred to as ECT active centers for HER/OER. Obviously,  $\text{Co}^{3+}$  cations are used in the position of  $\text{B}^{3+}$  and the double metal oxide expression changes to  $\text{MCo}_2\text{O}_4$ . Hyunsik Im et al. demonstrated that  $\text{CuCo}_2\text{O}_4$  is an efficient OER ECS in strong alkaline KOH media [17]. Unfortunately, its rate and cycle stability are hampered by low electrical conductivity. It has been proven that the mechanical and thermal stability of metal sulfides, rather than metal oxides, benefit from their diversified stoichiometry and crystal structures [18]. In plentiful chalcogenides, bimetallic sulfides ( $\text{MCo}_2\text{S}_4$ ) have been identified as the most promising catalysts, owing to the synergistic effect of two different metal ions. They exhibited excellent catalysis and have a richer redox state for many chemical conversions compared to monometallic sulfides and their electrical conductivity is also greater. Arumugam S. et al. [19] fabricated  $\text{NiCo}_2\text{S}_4$  for OER/HER with excellent activity and stability compared to  $\text{Ni}_3\text{S}_2$  and  $\text{NiCo}_2\text{O}_4$ , which is consistent with the above description. Moreover,  $\text{Ni}^{2+}$  and  $\text{Co}^{3+}$  metal ions occupy tetrahedral and octahedral positions, respectively, which surround a close-range sulfide ion. Zhu et al. [20] reported that  $\text{NiCo}_2\text{S}_4$  possesses an extremely small energy band and that its conductivity is much better than  $\text{NiCo}_2\text{O}_4$  (about 100 times) and single-metal oxides (about four-order of magnitude higher). Zhang et al. [21] reported that  $\text{NiCo}_2\text{S}_4$  has more octahedral catalytic active sites of  $\text{Co}^{3+}$  than the  $\text{NiCo}_2\text{O}_4$  crystal structure. Sun et al. [22] reported that  $\text{CuCo}_2\text{S}_4$  exhibited high-efficiency OER properties in alkaline solutions. Hence,  $\text{MCo}_2\text{S}_4$  has a great potential for BF ECT activity. Hao et al. reported that a Fe ion in  $\text{MCo}_2\text{S}_4$  could provide better electrical conductivity, while the sulfur element in redox could provide a richer redox state and improve conductivity [23]. Promisingly, the Fe element in the earth's crust is abundant (reserves of non-precious metals in the earth's crust:  $\text{Fe} \gg \text{Ni} > \text{Cu} > \text{Co} > \text{Mo}$ ). Therefore, by benefiting from the high-efficiency synergy between the Co ion, Fe ion, and S ion, the FCS remains promising in the area of HER/OER. Moreover, it is very important to exploit a successful template for improved ECT activities, and Ni foam can be widely used as a template because it can provide more reactive sites to contact with electrolyte ions [19].

Herein, the FCS NWs/Ni was fabricated by a hydrothermal method followed by exclusive vulcanization. The as-fabricated FCS NWs/Ni foams were used as flexible electrodes for HER/OER. Moreover, we investigated the effects of the onset-potential, Tafel slope, and concentration of  $\text{OH}^-$  in HER/OER. As a result, the FCS NWs/Ni showed splendid ECT activity for both HER and OER. Our work provides an interesting route to designing and fabricating stable and efficient ECS based on non-precious metals for OER/HER.

## 2. Experimental Section

### 2.1. Materials Preparation

The chemical reagents used in the experiments are shown in Table 1. All experiments were carried out under the surrounding experimental conditions. In addition, the cleaning method of the Ni foam substrate is consistent with the previous work of our research group [24].

**Table 1.** Reagents used during the experiment.

Agents	Company
$\text{Co}(\text{NO}_3)_2 \cdot 6\text{H}_2\text{O}$	Xilong Chemical Co., Ltd.
$\text{NH}_4\text{F}$	Xilong Chemical Co., Ltd.
Urea	Xilong Chemical Co., Ltd.
$\text{Fe}(\text{NO}_3)_3 \cdot 9\text{H}_2\text{O}$	Chengdu Kelong Chemical Co., Ltd.
$\text{Na}_2\text{S}$	Chengdu Kelong Chemical Co., Ltd.
HCl (34 wt%–37 wt%)	Alfa Aesar (Tianjin) Reagent Co., Ltd.
Acetone	Alfa Aesar (Tianjin) Reagent Co., Ltd.
KOH (AR)	Alfa Aesar (Tianjin) Reagent Co., Ltd.

All the other reagents with analytical purity were used in the synthesis process without further purification.

## 2.2. Synthesis Process

The FCS NWs/Ni was synthesized with a brief hydrothermal method [24].  $\text{Co}(\text{NO}_3)_2 \cdot 6\text{H}_2\text{O}$  (0.9 mmol) and  $\text{Fe}(\text{NO}_3)_3 \cdot 9\text{H}_2\text{O}$  (0.18 mmol) were dissolved in deionized water (30 mL) and dispersed uniformly by magnetic stirring. Then  $\text{NH}_4\text{F}$  (2.7 mmol) and urea (2.7 mmol) were added to the mixture while it was still being stirred. After stirring for 0.5 h, the solution was transferred into an autoclave and then the dried Ni foam was soaked in it. The sealed autoclave was put into a hydrothermal oven, maintained at 120 °C for 14 h. Afterward, the sample was cleaned carefully with acetone, alcohol, and ultrapure water several times (all about 30 mL each time), and then placed in a vacuum oven (60 °C for 12 h). The dried Ni foam was immersed into 0.1 M  $\text{Na}_2\text{S}$  solutions, sealed, and placed into a hot-air oven (120 °C for 10 h). After the vulcanization, the sample was carefully taken out and cleaned in the same way as previously mentioned. Eventually, the dried sample was obtained from a vacuum oven (60 °C after 12 h).

## 2.3. Characterization and Electrochemical Measurements

The microscopic morphologies of the FCS NWs/Ni were revealed by scanning electron microscopy (SEM, VEGA3 SBH, Tescan, Brno, Czech Republic). The X-ray diffraction (XRD) patterns were performed using Kratos Analytical Ltd. (Cu K $\alpha$  radiation, D/MAX-2500). The entire electrochemical test was performed in a three-electrode system with various concentrations of KOH electrolyte (0.05 M, 0.1 M, 0.2 M, and 1 M), using an electrochemical workstation (CHI660D, CH Instruments, Inc., Austin, TX, USA). The as-prepared FCS NWs/Ni foam acted as the working electrode, the saturated calomel electrode (SCE) was used as the reference electrode, and the platinum plate was used as the cathode. During the test process, the electrolyte was stirred with a magnet while slowly introducing nitrogen. The LSV (linear sweep voltammetry) of the as-fabricated FCS NWs/Ni was tested at a scan rate of 10 mV s<sup>-1</sup>. Electrochemical Impedance Spectrum (EIS) tests were carried out by applying an alternating current voltage with 5 mV perturbation amplitude and a frequency range from 100 kHz to 0.005 Hz. The chronopotentiometric measurements were used to test its long-term durability. Furthermore, the electrode potential could be transformed into the RHE (reversible hydrogen electrode) potential, which is related to the Nernst equation (the details were in Table 2).

**Table 2.** The electrode potential versus the SCE transferred to the RHE (reversible hydrogen electrode) potential.

The Nernst equation: E (vs. RHE) = E (vs. SCE) + E <sub>SCE</sub> + 0.0591 pH = E (SCE) + 0.241 + 0.0591 pH		
Electrolyte (M/KOH)	pH	E (RHE)
0.05	12.8	E (SCE) + 0.99748 V
0.1	13	E (SCE) + 1.0093 V
0.2	13.3	E (SCE) + 1.02703 V
1	14	E (SCE) + 1.0684 V

## 3. Results and Discussion

### 3.1. Morphology and Microstructure Characterization

The crystallinity of the FCS NWs/Ni was characterized via XRD. In Figure 1a, the diffraction peaks at 44.5° and 51.8° respond to the crystal orientations of Ni (111) and (200), respectively (JCPDS 04-0850). The 22.28°, 31.58°, 38.18°, 50.26°, and 55.92° diffraction peaks are in agreement with the characteristic peak of FCS [25,26]. Simultaneously, the typical XRD patterns of the precursor of FCS ( $\text{FeCo}_2(\text{C}_2\text{O}_4)_3$ ) possess three strong diffraction peaks (ranging from 30° to 40°) which are consistent with the reported literature [20]. SEM images of FCS NWs/Ni are shown in Figure 1b–d. Figure 1d displays the entire surface of the Ni foam. It was evenly covered by numerous FCS NWs. This nanostructure possesses two advantages: (i) it better penetrates the electrolyte and (ii) it provides a large specific

surface area. Thus, the transmission of electrons and ions between the nanowires and the conductive substrate can be greatly improved.

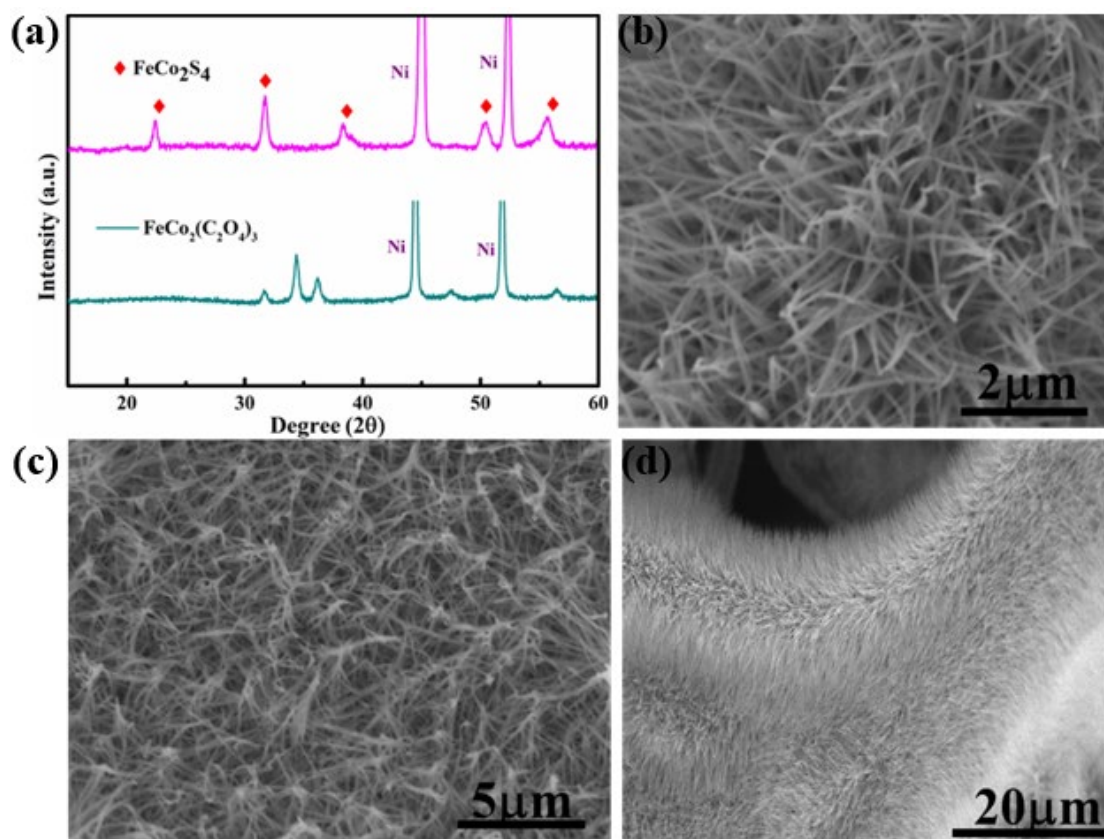
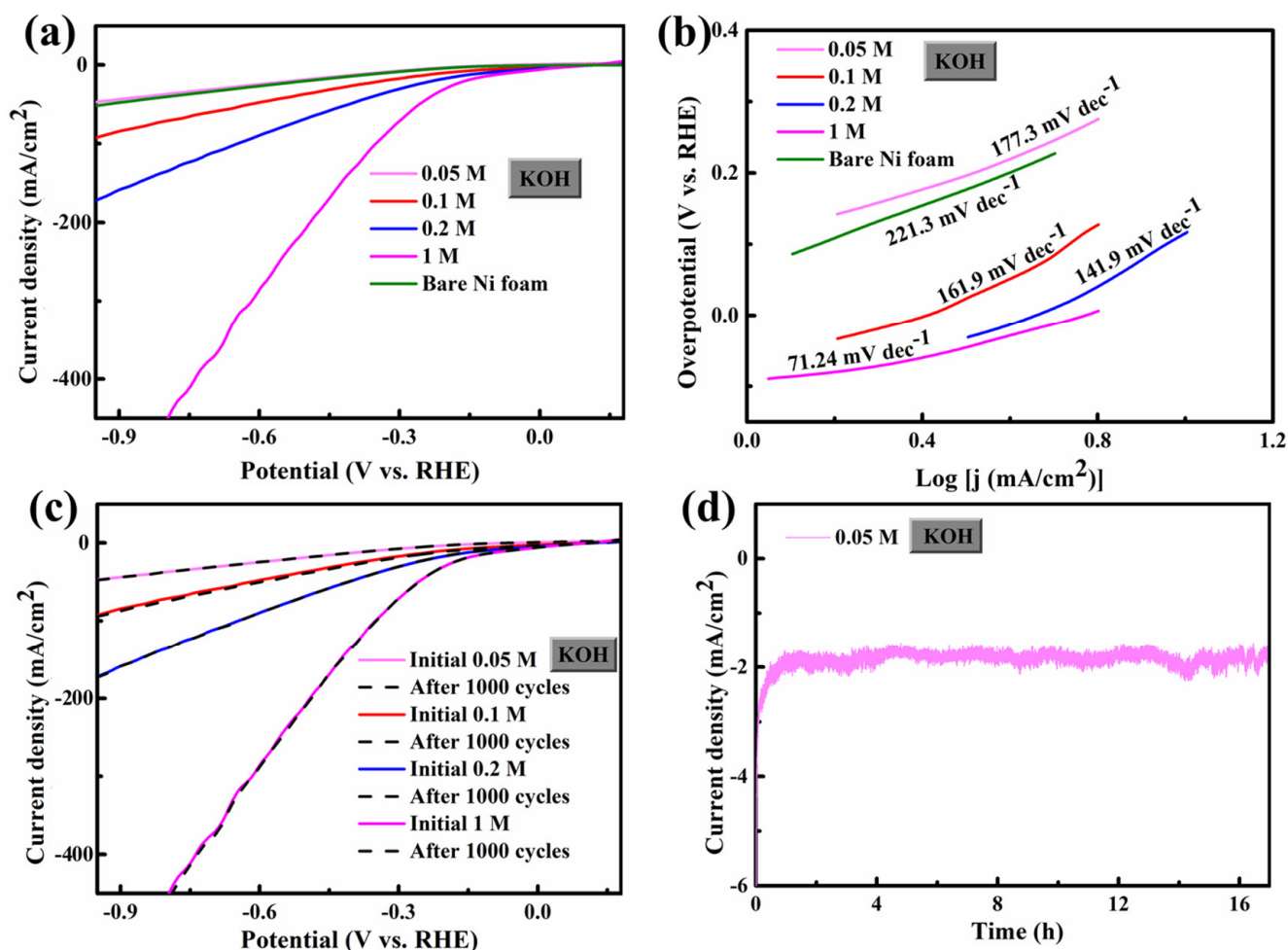


**Figure 1.** (a) XRD patterns of the  $\text{FeCo}_2\text{S}_4$  nanowire and the precursor of  $\text{FeCo}_2\text{S}_4$  ( $\text{FeCo}_2(\text{C}_2\text{O}_4)_3$ ). (b–d) SEM images of the  $\text{FeCo}_2\text{S}_4$  nanowire with different magnifications.

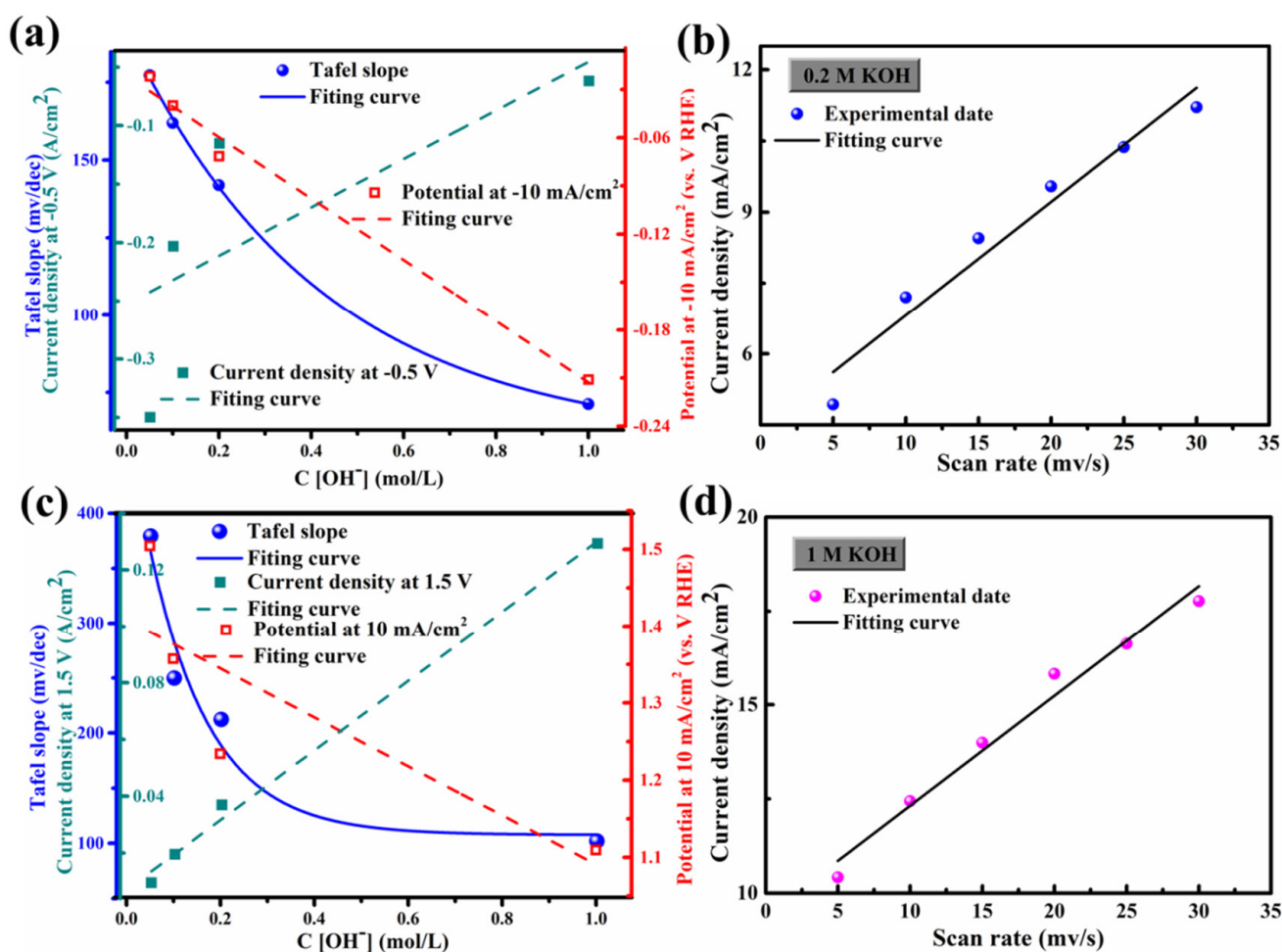
### 3.2. HER/OER Performance

Interestingly, since Ni foam has excellent conductivity, FCS NWs/Ni can be used as an electrode for HER and OER. The geometric surface area of these electrodes was  $1 \times 1 \text{ cm}^2$ . The electrocatalytic HER activity of the FCS NWs/Ni was assessed in a KOH solution with high-purity  $\text{N}_2$  and magnetic stirring. Figure 2a demonstrates the polarization curves with a scan of  $10 \text{ mV s}^{-1}$ . The cathode current of each sample was dramatically increased by increasing the negative potential. As shown in Figure 2a, the FCS NWs/Ni can provide an extraordinarily low overpotential ( $\eta$ ) of 62.6 mV (1 M KOH) with a current density of  $-10 \text{ mA cm}^{-2}$ . Meanwhile, the tests of FCS NWs/Ni were conducted at  $-10 \text{ mA cm}^{-2}$  under 0.05 M, 0.1 M, and 0.2 M KOH environments; the overpotential was 350.5 mV, 203.7 mV, and 115.97 mV, respectively. For comparison, the overpotential of the bare Ni foam was 328.5 mV ( $-10 \text{ mA cm}^{-2}$ , 0.05 M KOH). While the cathodic current density achieved  $-20 \text{ mA cm}^{-2}$ , the FCS NWs/Ni foam in 1 M KOH only required an overpotential of 158.6 mV, smaller than 524.5 mV (0.05 M), 334.7 mV (0.1 M), and 227.97 mV (0.2 M). The Tafel slope is dependent on the intrinsic kinetics of the catalyst, as shown in Figure 2b. Generally, a smaller Tafel slope indicates that a higher current density can be achieved at a lower overpotential [27]. The Tafel slope  $b$  can be obtained by the equation [28]:  $\eta = a + b \log j$ . Interestingly, the FCS NWs/Ni electrode shows a Tafel slope of  $71.24 \text{ mV dec}^{-1}$  (1 M KOH), which is much lower than that in 0.05 M KOH ( $177.3 \text{ mV dec}^{-1}$ ), 0.1 M KOH ( $161.9 \text{ mV dec}^{-1}$ ), 0.2 M KOH ( $141.9 \text{ mV dec}^{-1}$ ), and the bare Ni foam in 0.05 M KOH ( $221.3 \text{ mV dec}^{-1}$ ). The performance of the FCS NWs/Ni electrode is much better than most HER electrocatalysts, which were reported previously, in KOH solutions (Table 3). In addition, the inherent HER performance of FCS NWs/Ni is regulated by the  $\text{OH}^-$

concentration. Meanwhile, typical HER results in different concentrations of  $\text{OH}^-$  ( $\text{C}[\text{OH}^-]$ ) were summarized and compared in Figure 3a. It is revealed that with the improvement of  $\text{C}[\text{OH}^-]$ , the HER property is greatly enhanced. The higher electrocatalytic performance of the FCS NWs/Ni is mainly attributed to the remarkable synergy between Co, Fe, and S, and that the Ni foam can promote the entry of electrolyte ions at the active site [19]. Hence, the small Tafel slope and the low HER onset potential suggest that FCS NWs/Ni is a qualified candidate to act as an HER electrocatalyst [29]. The ADT (accelerated durability tests) of FCS NWs/Ni in KOH solutions with various concentrations were tested at the same scan rate of  $100 \text{ mV s}^{-1}$  for 1000 cycles. In Figures 2c and 4, we can see that the polarization curves of FCS NWs/Ni have almost no obvious attenuation after 1000 cycles. Compared to other concentrations of KOH electrolytes, the polarization curve for the 0.1 M KOH electrolyte exhibited a more noticeable divergence (Figure 4b). This divergence can be attributed to the accidental shedding of the active material during HER reaction. In addition, as shown in Figure 2d, the cathodic current density for the FCS NWs/Ni catalyst achieves a small degradation after 17 h in 0.05 M KOH with a  $-0.8 \text{ V}$  overpotential.

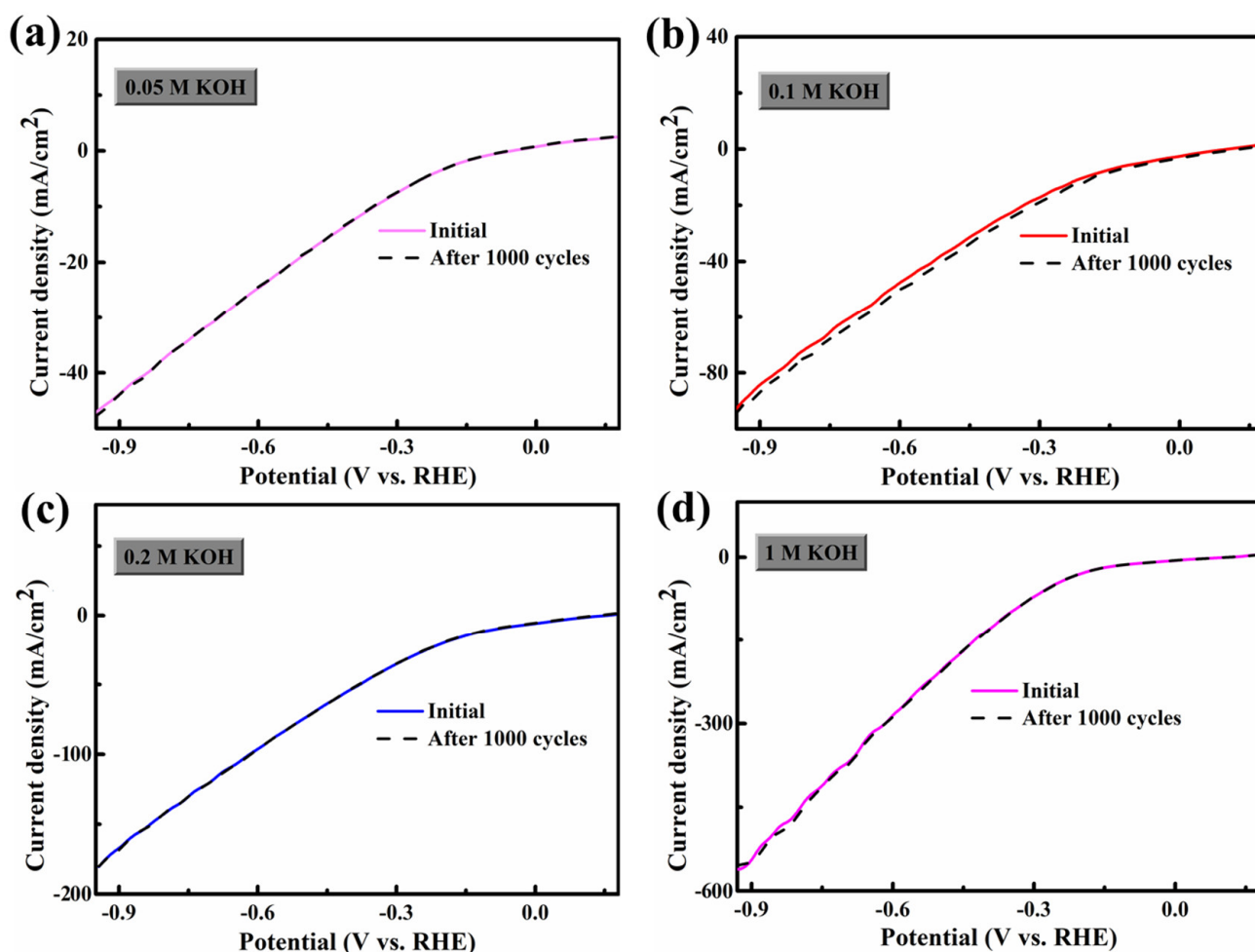


**Figure 2.** (a) Polarization curves obtained with bare Ni foam in 0.05 M KOH and FeCo<sub>2</sub>S<sub>4</sub> nanowire in different electrolytes (0.05, 0.1, 0.2, and 1 M KOH); (b) the bare Ni foam and FeCo<sub>2</sub>S<sub>4</sub> nanowires corresponding to Tafel diagrams; (c) photozation curves of the initial LSV polarization curve of FeCo<sub>2</sub>S<sub>4</sub> nanowires after 1000 cycles; and (d) the chronoamperometric response of a FeCo<sub>2</sub>S<sub>4</sub> nanowire at a constant potential of  $-0.8 \text{ V}$ . All experiments were conducted for HER.



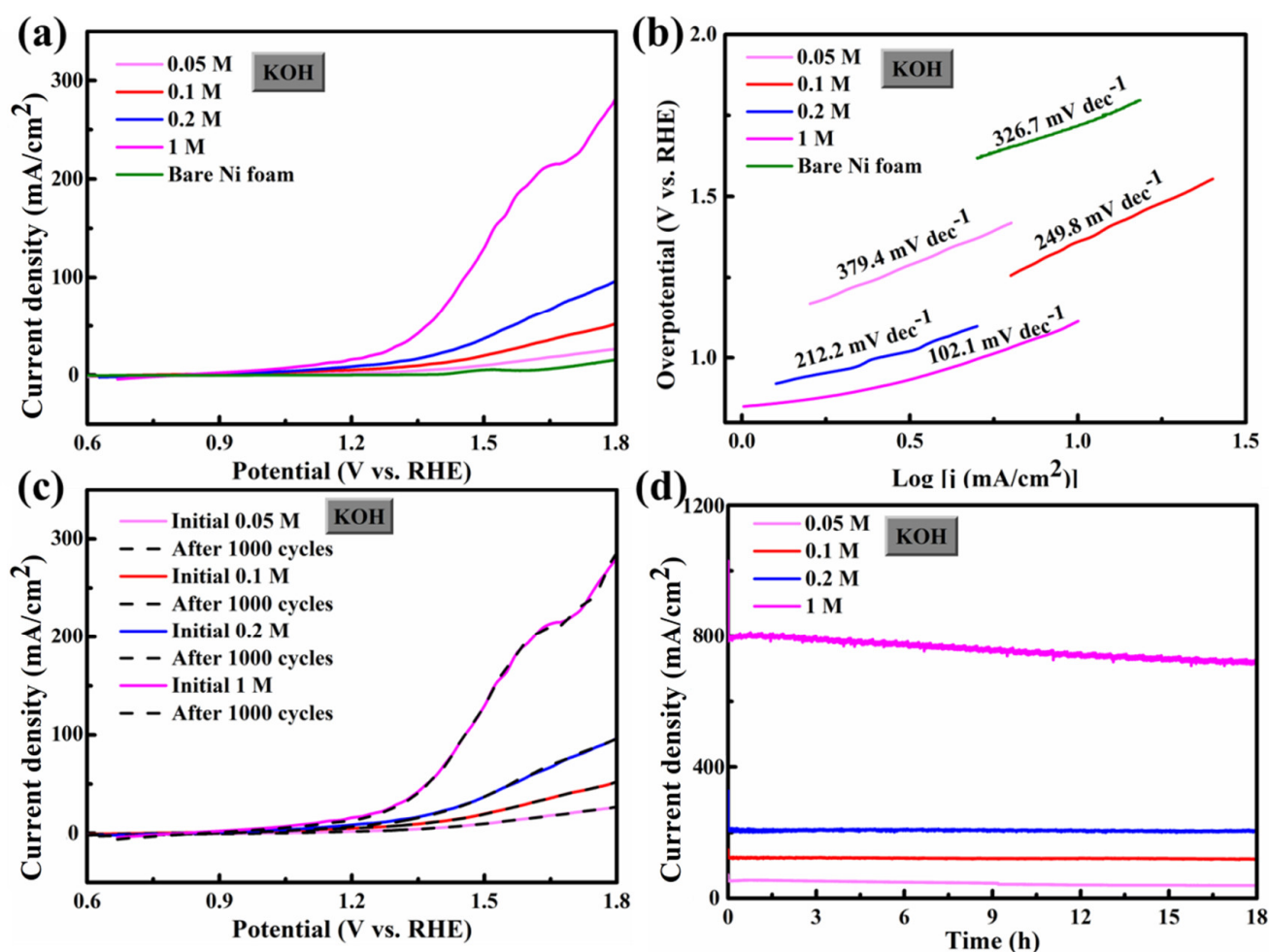
**Figure 3.** (a) The current density of  $-10 \text{ mA/cm}^2$  and the Tafel slope calculated at a potential of  $-0.5 \text{ V}$ , which is used as a function of the concentration of  $\text{OH}^-$  ( $C[\text{OH}^-]$ ) with all experiments were performed for HER; (b) The current density at  $1.25 \text{ V}$  vs. RHE of  $\text{FeCo}_2\text{S}_4$  nanowire in  $0.2 \text{ M KOH}$ ; (c) the slope of Tafel of  $10 \text{ mA/cm}^2$  current density and  $1.5 \text{ V}$  potential calculated as a function of the concentration of  $\text{OH}^-$  ( $C[\text{OH}^-]$ ); all experiments were conducted for OER; and (d)  $1 \text{ M KOH}$  achieved at different scan ( $5, 10, 15, 20, 25,$  and  $30 \text{ mV/s}$ ).

The test conditions for the OER activity of FCS NWs/Ni are the same as those for HER. Figure 5a shows that the FCS NWs/Ni has a low overpotential ( $\eta$ ) of  $1.11 \text{ V}$  ( $10 \text{ mA cm}^{-2}$  in  $1 \text{ M KOH}$ ); it is obviously lower than  $1.51 \text{ V}$  ( $0.05 \text{ M}$ ),  $1.36 \text{ V}$  ( $0.1 \text{ M}$ ),  $1.24 \text{ V}$  ( $0.2 \text{ M}$ ), and  $1.72 \text{ V}$  (bare Ni foam in  $0.05 \text{ M KOH}$ ). Furthermore, it is lower than most of the other OER electrocatalysts, which were reported previously (as shown in Table 3). When the current density of the FCS NWs/Ni electrode increased to  $20 \text{ mA cm}^{-2}$  in  $1 \text{ M KOH}$ , the overpotential was only  $1.25 \text{ V}$ , which is lower than  $1.69 \text{ V}$  ( $0.05 \text{ M}$ ),  $1.50 \text{ V}$  ( $0.1 \text{ M}$ ), and  $1.38 \text{ V}$  ( $0.2 \text{ M}$ ). The peak of bifunctional activity is influenced by the octahedral centers of the electrocatalyst [15]. In tetrahedrons and octahedrons, a dense array of large  $\text{S}^{2-}$  anions with iron and cobalt metal cations allows FCS NW to have excellent performance at the active octahedral position of the  $\text{Co}^{3+}$  cation [21]. Nevertheless, FCS showed a significant oxidation peak at  $1.6 \text{ V}$  (vs. RHE) which can be attributed to the surface reaction, as shown in the following equation.



**Figure 4.** Polarization curves for  $\text{FeCo}_2\text{S}_4$  nanowire with an initial LSV polarization curve after 1000 cycles in different electrolytes: (a) 0.05 M KOH, (b) 0.1 M KOH, (c) 0.2 M KOH, and (d) 1 M KOH. All experiments were carried out for HER.

The Tafel slope was used to assess OER kinetics, as shown in Figure 5b. The Tafel slope of FCS NWs/Ni in 1 M KOH was  $102.1 \text{ mV dec}^{-1}$ , smaller than the electrode in all other electrolytes (0.05 M:  $379.4 \text{ mV dec}^{-1}$ , 0.1 M:  $249.8 \text{ mV dec}^{-1}$ , and 0.2 M:  $212.2 \text{ mV dec}^{-1}$ ), including bare Ni foam in 0.05 M KOH ( $326.7 \text{ mV dec}^{-1}$ ). The smaller Tafel slope also indicates the efficient electron and ion transform. The ADT test conditions of FCS NWs/Ni for the OER are the same as for the HER. In Figure 5c, the polarization curves of the FCS anodic current almost have no reduction after 1000 cycles. Figure 5d showed the chronoamperometric response of  $\text{FeCo}_2\text{S}_4$  at a constant applied potential (0.8 V). After 18 h of testing, there was only a slight decrease in current density. As for the case of 1 M KOH electrolyte, the current density decreased by about 8.5%, which might result from the irreversible phase transformation of metal sulfides to metal oxide/oxyhydroxide [26,30]. Furthermore, the intrinsic OER properties of FCS were affected by the concentration of  $\text{OH}^-$  (Figure 3c). The OER performance was hugely improved with increased  $\text{C}[\text{OH}^-]$ ; the required overpotential changed almost linearly with  $\text{C}[\text{OH}^-]$ .

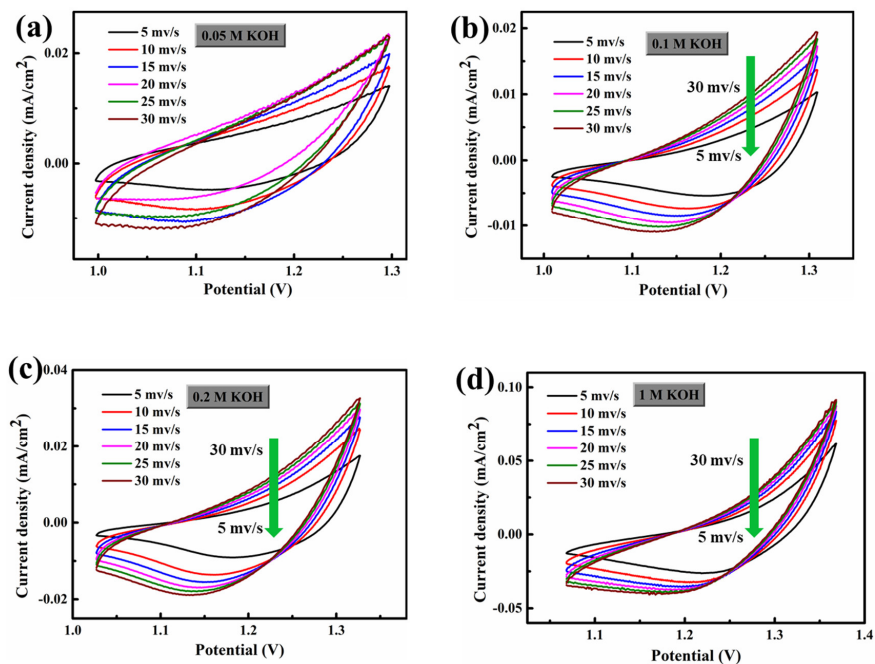
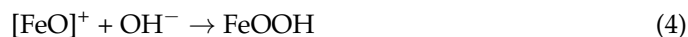
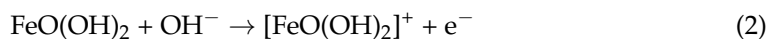
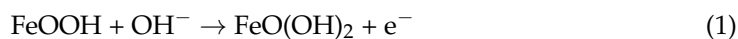


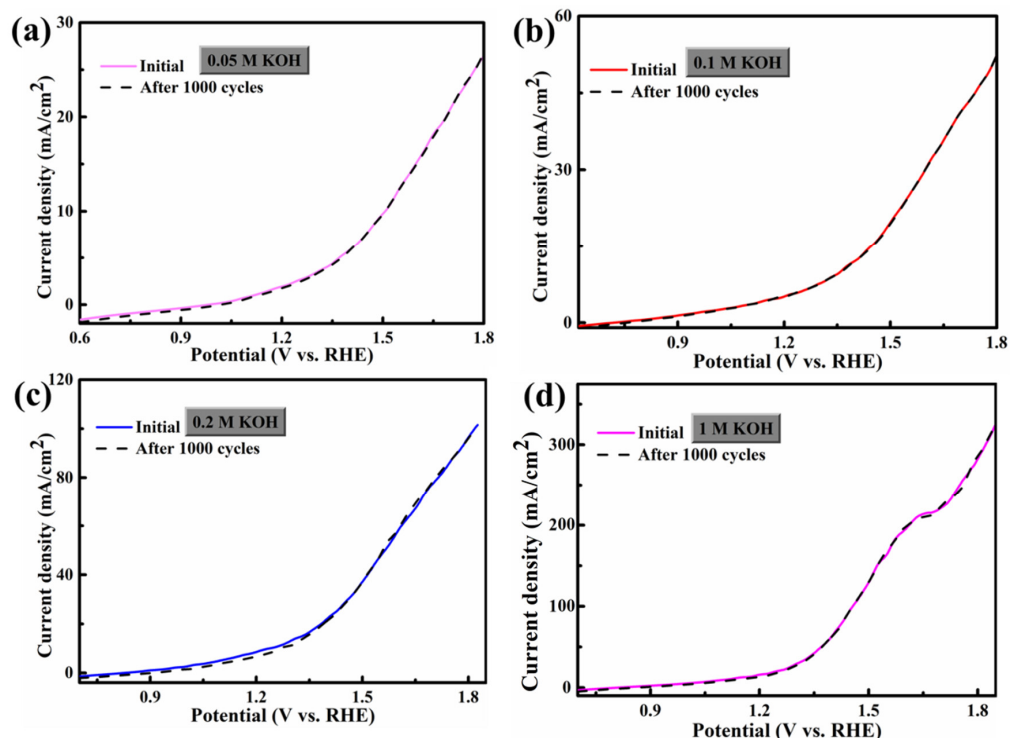
**Figure 5.** (a) LSV curves for  $\text{FeCo}_2\text{S}_4$  nanowire and bare Ni foam for OER in 0.05, 0.1, 0.2, 1 M KOH; (b) The corresponding Tafel plots; (c) Polarization curves for  $\text{FeCo}_2\text{S}_4$  nanowire with an initial LSV polarization curve after 1000 cycles; and (d) the chronoamperometric response kept an account of  $\text{FeCo}_2\text{S}_4$  at a constant applied potential (0.8 V).

Figure 6 shows the CV (cyclic voltammetric) curves of FCS NWs/Ni electrolytes in 0.05 M, 0.1 M, 0.2 M, and 1 M KOH. The scanning rates were from  $5 \text{ mV s}^{-1}$  to  $30 \text{ mV s}^{-1}$ . The distorted rectangular-like shape of FCS NWs/Ni was similar to  $\text{NiCo}_2\text{S}_4$  reported previously in the literature [20]. Furthermore, the CV curve remained in good shape, indicating that the electron and ion transfer rates are fast enough [31]. In Figure 3b,d, we can see that the fitting curve of FCS NWs/Ni at the potential of 1.25 vs. RHE (in 0.2 M and 1 M KOH) with different scan rates ( $5, 10, 15, 20, 25,$  and  $30 \text{ mV s}^{-1}$ ). These excellent properties indicate that FCS NWs/Ni has great potential for application in OER. The remarkable conductivity represents a fast electron transfer rate and accelerated reaction kinetics. Figure 7 showed the Polarization curves for the  $\text{FeCo}_2\text{S}_4$  nanowire with an initial LSV polarization curve and after 1000 cycles. The curves almost overlapped completely, indicating the stability of OER performance of the  $\text{FeCo}_2\text{S}_4$  nanowire. The EIS measurements of FCS NWs/Ni were conducted, in 0.05 M, 0.1 M, 0.2 M, and 1 M KOH, as shown in Figure 8. Figure 8a–c, reveals that the  $\text{FeCo}_2\text{S}_4$  in 1 M KOH had a smaller EIS compared to the three other concentrations of KOH solution and that it increased slightly after cycling. In addition, as shown in Figure 8d, the current density curve had a small attenuation at an overpotential of 0.8 V (0.1 M KOH). Therefore, all the above results reveal that the hybrid structure of FCS NWs/Ni has stupendous potential in the overall water-splitting field.

**Table 3.** The performance of the FeCo<sub>2</sub>S<sub>4</sub> electrode compared with the OER/HER electrocatalysts reported previously in KOH solutions.

	Materials	Electrolyte	J (mA/cm <sup>2</sup> )	Overpotential (V)	Tafel Slope (mV dec <sup>-1</sup> )	References
HER	FeCo <sub>2</sub> S <sub>4</sub> /Ni foam	1 M KOH	10	0.0626	71.24	This work
		0.2 M KOH	10	0.11597	141.9	
		0.1 M KOH	10	0.2037	161.9	
		0.05 M KOH	10	0.35052	177.3	
		1 M KOH	10	1.1124	102.1	
OER	FeCo <sub>2</sub> S <sub>4</sub> /Ni foam	0.2 M KOH	10	1.237	212.2	This work
		0.1 M KOH	10	1.3603	249.8	
		0.05 M KOH	10	1.50748	379.4	
		1 M KOH	10	0.097	79	
HER/ OER	Ni <sub>3</sub> Se <sub>2</sub> /Ni foam	1 M KOH	100	0.353	144	[32]
HER/ OER	NiSe <sub>2</sub> NSs-120	1 M KOH	10	0.207	186.5	[33]
		1 M KOH	40	1.562	109.4	
HER/ OER	NiCo <sub>2</sub> S <sub>4</sub> /CC	1 M KOH	50	0.263	141	[34]
		1 M KOH	50	0.31	89	
OER	CuCo <sub>2</sub> O <sub>4</sub>	1 M KOH	20	0.29	117	[17]
HER	CoOx@CN	1 M KOH	10	0.232	...	[35]
OER	FeCoW oxyhydroxides	1 M KOH	10	0.191	...	[36]
HER	β-InSe	1 M KOH	10	0.483	135	[37]
OER	CuCo <sub>2</sub> S <sub>4</sub> /CF	1 M KOH	60	0.259	110	[38]
HER/ OER	NiSe <sub>2</sub> NCs	1 M KOH	10	0.54	139	[39]
		1 M KOH	10	0.25	38	

**Figure 6.** Electrochemical cycle voltammograms of the FeCo<sub>2</sub>S<sub>4</sub> nanowire in different electrolytes (a) 0.05 M KOH, (b) 0.1 M KOH, (c) 0.2 M KOH, and (d) 1 M KOH under the conditions of different potential scanning rates. The potential range of the selected no-faradic current was 0–0.3 V.



**Figure 7.** Polarization curves for the FeCo<sub>2</sub>S<sub>4</sub> nanowire with an initial LSV polarization curve after 1000 cycles in different electrolytes: (a) 0.05 M KOH, (b) 0.1 M KOH, (c) 0.2 M KOH, and (d) 1 M KOH. All experiments were carried out for OER.

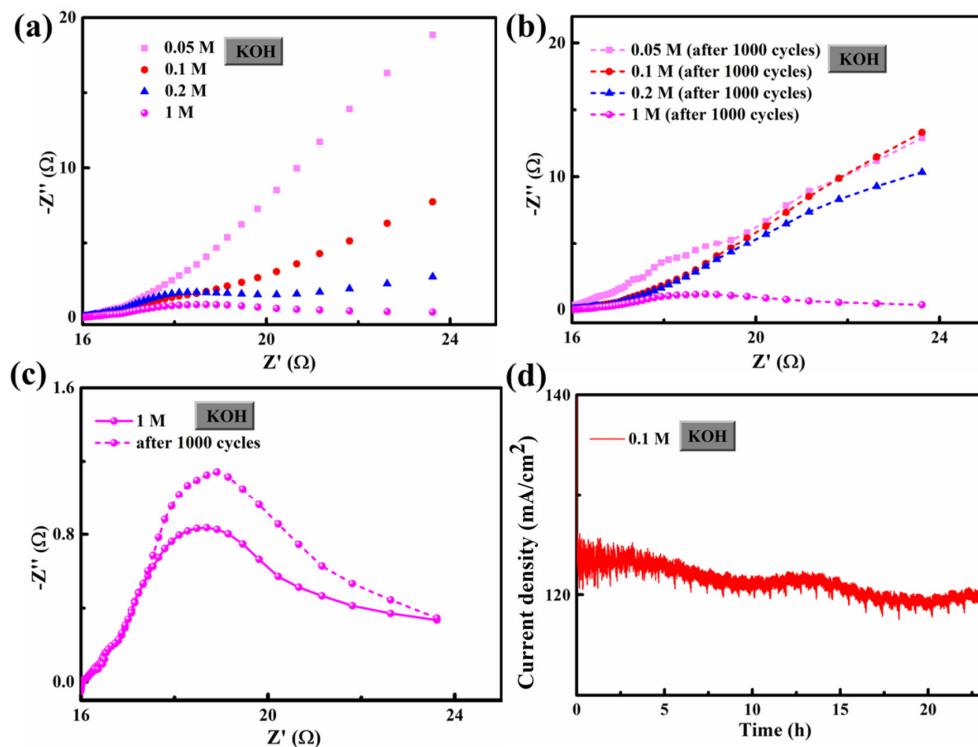


**Figure 8.** (a) Initial and (b) after 1000 cycles electrochemical impedance spectra of FeCo<sub>2</sub>S<sub>4</sub> nanowires in 0.05 M, 0.1 M, 0.2 M, and 1 M KOH at an applied potential (0.4 V); (c) electrochemical impedance spectra for FeCo<sub>2</sub>S<sub>4</sub> with initial curves and after 1000 cycles; and (d) the chronoamperometric response kept an account of FeCo<sub>2</sub>S<sub>4</sub> at a constant applied potential of 0.8 V (0.1 M KOH).

#### 4. Conclusions

In this study, a smart FCS NWs/Ni hybrid structure was prepared as a non-noble metal electrocatalyst in different alkaline solutions for OER/HER. The unique design of the microstructure endowed the FCS NWs/Ni with a high ion/electron transport capacity and a large specific surface area. Moreover, its excellent conductivity, higher specific capacity, and rich redox state are attributed to its iron, cobalt, and sulfur elements, respectively. The FCS NWs/Ni catalysts achieved  $10 \text{ mA cm}^{-2}$  at HER overpotential of 62.6 mV (1 M KOH) and  $129.56 \text{ mA cm}^{-2}$  at OER overpotential of 1.5 V (1 M KOH). Lastly, the method presented in this work will instruct the future reasonable design and development of efficient bifunctional non-precious metal electrocatalysts to be widely used in the field of electrochemical hydrogen and oxygen production in water electrolytic systems.

**Author Contributions:** J.T. contributed to the experiment and wrote the paper; the data was processed and analyzed by S.L. (Shuhua Liu), Y.L. (Yanmo Liao), H.Q. and Y.W.; Y.L. (Yu Liu), H.C., M.T. and S.L. (Sanjie Liu) conducted the experiment and discussed the results; Z.Q., C.L. and X.Q. proposed the study conception and were responsible for part of the experimental data, data discussion, and grammar revision. All authors have read and agreed to the published version of the manuscript.

**Funding:** This work was supported by the National Natural Science Foundation of China (No. 11504312), the Provincial Natural Science Foundation of Hunan (No. 2021JJ30298), the Science and Technology Program of Hunan Province, China (Grant No. 2019TP1014), and the Changjiang Scholars and Innovative Research Team in University (IRT\_17R91).

**Institutional Review Board Statement:** Not applicable.

**Informed Consent Statement:** Not applicable.

**Data Availability Statement:** The data presented in this study are available on request from the corresponding author.

**Conflicts of Interest:** The authors declare no conflict of interest.

#### References

1. Guo, Y.; Park, T.; Yi, J.W.; Henzie, J.; Kim, J.; Wang, Z.; Jiang, B.; Bando, Y.; Sugahara, Y.; Tang, J. Nanoarchitectonics for Transition-Metal-Sulfide-Based Electrocatalysts for Water Splitting. *Adv. Mater.* **2019**, *31*, 1807134. [[CrossRef](#)] [[PubMed](#)]
2. Xi, X.; Wang, X.W.; Fan, Y.; Wang, Q.; Lu, Y.; Li, J.; Shao, L.; Luo, J.L.; Fu, X.Z. Efficient bifunctional electrocatalysts for solid oxide cells based on the structural evolution of perovskites with abundant defects and exsolved CoFe nanoparticles. *J. Power Sources* **2021**, *482*, 228981. [[CrossRef](#)]
3. Lei, Z.; Wang, T.; Zhao, B.; Cai, W.; Liu, Y.; Jiao, S.; Li, Q.; Cao, R.; Liu, M. Recent Progress in Electrocatalysts for Acidic Water Oxidation. *Adv. Energy Mater.* **2020**, *10*, 2000478. [[CrossRef](#)]
4. Luo, Y.; Zhou, H.; Sun, J.; Fan, Q.; Dan, L.; Xie, L.; Fang, Y.; Bao, J.; Yong, L.; Ying, Y. Hierarchical Cu@CoFe layered double hydroxide core-shell nanoarchitectures as bifunctional electrocatalysts for efficient overall water splitting. *Nano Energy* **2017**, *41*, 327–336.
5. Ledendecker, M.; Krick Calderón, S.; Papp, C.; Steinrück, H.P.; Antonietti, M.; Shalom, M. The Synthesis of Nanostructured Ni<sub>5</sub>P<sub>4</sub> Films and their Use as a Non-Noble Bifunctional Electrocatalyst for Full Water Splitting. *Angew. Chem. Int. Ed.* **2015**, *54*, 12361–12365. [[CrossRef](#)]
6. Wang, B.; Ye, Y.; Xu, L.; Quan, Y.; Wei, W.; Zhu, W.; Li, H.; Xia, J. Space-Confined Yolk-Shell Construction of Fe<sub>3</sub>O<sub>4</sub> Nanoparticles Inside N-Doped Hollow Mesoporous Carbon Spheres as Bifunctional Electrocatalysts for Long-Term Rechargeable Zinc-Air Batteries. *Adv. Funct. Mater.* **2020**, *30*, 2005834. [[CrossRef](#)]
7. Zhang, C.; Liu, J.; Ye, Y.; Aslam, Z.; Brydson, R.; Liang, C. Fe-N-Doped Mesoporous Carbon with Dual Active Sites Loaded on Reduced Graphene Oxides for Efficient Oxygen Reduction Catalysts. *ACS Appl. Mater. Interfaces* **2018**, *10*, 2423–2429. [[CrossRef](#)]
8. Luque-Centeno, J.M.; Martínez-Huerta, M.V.; Sebastián, D.; Lemes, G.; Pastor, E.; Lázaro, M.J. Bifunctional N-doped graphene Ti and Co nanocomposites for the oxygen reduction and evolution reactions. *Renew. Energy* **2018**, *125*, 182–192. [[CrossRef](#)]
9. Devaguptapu, S.V.; Hwang, S.; Karakalos, S.; Zhao, S.; Gupta, S.; Su, D.; Xu, H.; Wu, G. Morphology Control of Carbon-Free Spinel NiCo<sub>2</sub>O<sub>4</sub> Catalysts for Enhanced Bifunctional Oxygen Reduction and Evolution in Alkaline Media. *ACS Appl. Mater. Interfaces* **2018**, *9*, 44567–44578. [[CrossRef](#)]
10. Liu, K.; Li, J.; Li, J.; Wang, J.; Zhao, D.; Jiang, J.; Qian, D. A facile and low-cost synthesis of MnO<sub>x</sub>/Mn<sub>2</sub>N-N-C nanohybrid as an advanced oxygen reduction electrocatalyst. *Mater. Res. Bull.* **2018**, *104*, 60–64. [[CrossRef](#)]
11. Wang, D.; Luo, D.; Zhang, Y.; Zhao, Y.; Zhou, G.; Shui, L.; Chen, Z.; Wang, X. Deciphering interpenetrated interface of transition metal oxides/phosphates from atomic level for reliable Li/S electrocatalytic behavior. *Nano Energy* **2021**, *81*, 105602. [[CrossRef](#)]

12. Zhou, Y.; Xi, S.; Wang, J.; Sun, S.; Wei, C.; Feng, Z.; Du, Y.; Xu, Z.J. Revealing the Dominant Chemistry for Oxygen Reduction Reaction on Small Oxide Nanoparticles. *ACS Catal.* **2017**, *8*, 673–677. [[CrossRef](#)]
13. Ting, B.; Hui, Z.; Jiang, Y.; Jin, C.; Wu, J.; Hong, Y.; Deren, Y. Epitaxial Growth of Twinned Au-Pt Core-Shell Star-Shaped Decahedra as Highly Durable Electrocatalysts. *Nano Lett.* **2015**, *15*, 7808–7815.
14. Wu, X.; Niu, Y.; Feng, B.; Yu, Y.; Huang, X.; Zhong, C.; Hu, W.; Li, C.M. Mesoporous Hollow Nitrogen-Doped Carbon Nanospheres with Embedded MnFe<sub>2</sub>O<sub>4</sub>/Fe Hybrid Nanoparticles as Efficient Bifunctional Oxygen Electrocatalysts in Alkaline Media. *ACS Appl. Mater. Interfaces* **2018**, *10*, 20440–20447. [[CrossRef](#)] [[PubMed](#)]
15. Suntivich, J.; May, K.J.; Gasteiger, H.A.; Goodenough, J.B.; Shaohorn, Y. A Perovskite Oxide Optimized for Oxygen Evolution Catalysis from Molecular Orbital Principles. *Chem. Inform.* **2012**, *43*, 1383–1385. [[CrossRef](#)]
16. Hogg, S.A. Oxidation states of Co and Fe in Ba<sub>1-x</sub>Sr<sub>x</sub>Co<sub>1-y</sub>FeyO<sub>3-δ</sub> (x,y = 0.2–0.8) and oxygen desorption in the temperature range 300–1273 K. *Phys. Chem. Chem. Phys.* **2009**, *11*, 3090–3098.
17. Aqueel Ahmed, A.T.; Hou, B.; Chavan, H.S.; Jo, Y.; Cho, S.; Kim, J.; Pawar, S.M.; Cha, S.; Inamdar, A.I.; Kim, H. Self-Assembled Nanostructured CuCo<sub>2</sub>O<sub>4</sub> for Electrochemical Energy Storage and the Oxygen Evolution Reaction via Morphology Engineering. *Small* **2018**, *14*, 1800742. [[CrossRef](#)]
18. Shi, J.; Li, X.; He, G.; Zhang, L.; Li, M. Electrodeposition of high-capacitance 3D CoS/graphene nanosheets on nickel foam for high-performance aqueous asymmetric supercapacitors. *J. Mater. Chem. A* **2015**, *3*, 20619–20626. [[CrossRef](#)]
19. Sivanantham, A.; Ganesan, P.; Shanmugam, S. Bifunctional Electrocatalysts: Hierarchical NiCo<sub>2</sub>S<sub>4</sub> Nanowire Arrays Supported on Ni Foam: An Efficient and Durable Bifunctional Electrocatalyst for Oxygen and Hydrogen Evolution Reactions. *Adv. Funct. Mater.* **2016**, *26*, 4660. [[CrossRef](#)]
20. Zhu, J.; Tang, S.; Wu, J.; Shi, X.; Zhu, B.; Meng, X. Wearable High-Performance Supercapacitors Based on Silver-Sputtered Textiles with FeCo<sub>2</sub>S<sub>4</sub>@NiCo<sub>2</sub>S<sub>4</sub> Composite Nanotube-Built Multitripod Architectures as Advanced Flexible Electrodes. *Adv. Energy Mater.* **2017**, *7*, 1601234. [[CrossRef](#)]
21. Zhang, Z.; Wang, X.; Cui, G.; Zhang, A.; Zhou, X.; Xu, H.; Gu, L. NiCo<sub>2</sub>S<sub>4</sub> sub-micron spheres: An efficient non-precious metal bifunctional electrocatalyst. *Nanoscale* **2014**, *6*, 3540–3544. [[CrossRef](#)]
22. Yang, L.; Xie, L.; Ren, X.; Wang, Z.; Liu, Z.; Du, G.; Asiri, A.M.; Yao, Y.; Sun, X. Hierarchical CuCo<sub>2</sub>S<sub>4</sub> nanoarrays for high-efficient and durable water oxidation electrocatalysis. *Chem. Commun.* **2017**, *52*, 78–81. [[CrossRef](#)]
23. Hao, Z.; He, X.; Li, H.; Trefilov, D.; Song, Y.; Li, Y.; Fu, X.; Cui, Y.; Tang, S.; Ge, H. Vertically Aligned and Ordered Arrays of 2D MCo<sub>2</sub>S<sub>4</sub>@Metal with Ultrafast Ion/Electron Transport for Thickness-Independent Pseudocapacitive Energy Storage. *ACS Nano* **2020**, *14*, 12719–12731. [[CrossRef](#)] [[PubMed](#)]
24. Xu, G.; Zhang, Z.; Qi, X.; Ren, X.; Liu, S.; Chen, Q.; Huang, Z.; Zhong, J. Hydrothermally synthesized FeCo<sub>2</sub>O<sub>4</sub> nanostructures: Structural manipulation for high-performance all solid-state supercapacitors. *Ceram. Int.* **2018**, *4*, 120–127. [[CrossRef](#)]
25. Tang, S.; Zhu, B.; Shi, X.; Wu, J.; Meng, X. General Controlled Sulfidation toward Achieving Novel Nanosheet-Built Porous Square-FeCo<sub>2</sub>S<sub>4</sub>-Tube Arrays for High-Performance Asymmetric All-Solid-State Pseudocapacitors. *Adv. Energy Mater.* **2017**, *7*, 1601985. [[CrossRef](#)]
26. Huang, Y.; Chen, X.; Ge, S.; Zhang, Q.; Zhang, X.; Li, W.; Cui, Y. Hierarchical FeCo<sub>2</sub>S<sub>4</sub>@CoFe layered double hydroxide on Ni foam as bifunctional electrocatalyst for overall water splitting. *Catal. Sci. Technol.* **2020**, *10*, 1292–1298. [[CrossRef](#)]
27. Qiao, H.; Liu, H.; Huang, Z.; Ma, Q.; Luo, S.; Li, J.; Liu, Y.; Zhong, J.; Qi, X. Black Phosphorus Nanosheets Modified with Au Nanoparticles as High Conductivity and High Activity Electrocatalyst for Oxygen Evolution Reaction. *Adv. Energy Mater.* **2020**, *10*, 2002424. [[CrossRef](#)]
28. Jaramillo, T.F.; Jørgensen, K.P.; Bonde, J.; Nielsen, J.H.; Horch, S.; Chorkendorff, I. Identification of Active Edge Sites for Electrochemical H<sub>2</sub> Evolution from MoS<sub>2</sub> Nanocatalysts. *Science* **2007**, *317*, 100–102. [[CrossRef](#)]
29. Menezes, P.; Panda, C.; Loos, S.; Bunscheibruns, F.; Walter, C.; Schwarze, M.; Deng, X.; Dau, H.; Driess, M. A structurally versatile nickel phosphite acting as a robust bifunctional electrocatalyst for overall water splitting. *Energy Environ. Sci.* **2018**, *5*, 1287–1298. [[CrossRef](#)]
30. Zhang, H.; Li, X.; Hähnel, A.; Naumann, V.; Lin, C.; Azimi, S.; Schweizer, S.L.; Maijenburg, A.W.; Wehrspohn, R.B. Bifunctional Heterostructure Assembly of NiFe LDH Nanosheets on NiCoP Nanowires for Highly Efficient and Stable Overall Water Splitting. *Adv. Funct. Mater.* **2018**, *28*, 1706847. [[CrossRef](#)]
31. Liu, B.; Yang, M.; Yang, D.; Chen, H.; Li, H. Graphene-like porous carbon nanosheets for ultra-high rate performance supercapacitors and efficient oxygen reduction electrocatalysts. *J. Power Sources* **2020**, *456*, 227999. [[CrossRef](#)]
32. Xu, R.; Wu, R.; Shi, Y.; Zhang, J.; Zhang, B. Ni<sub>3</sub>Se<sub>2</sub> nanoforest/Ni foam as a hydrophilic, metallic, and self-supported bifunctional electrocatalyst for both H<sub>2</sub> and O<sub>2</sub> generations. *Nano Energy* **2016**, *24*, 103–110. [[CrossRef](#)]
33. Jie, Z.; Liu, Y.; Zhen, Z.; Huang, Z.; Chen, X.; Ren, X.; Long, R.; Xiang, Q.; Zhong, J. Hierarchical NiSe<sub>2</sub> sheet-like nano-architectures as an efficient and stable bifunctional electrocatalyst for overall water splitting: Phase and morphology engineering. *Electrochim. Acta* **2018**, *279*, 195–203.
34. Kang, J.; Wood, J.D.; Wells, S.A.; Lee, J.H.; Liu, X.; Chen, K.S.; Hersam, M.C. Solvent Exfoliation of Electronic-Grade, Two-Dimensional Black Phosphorus. *ACS Nano* **2015**, *9*, 3596–3604. [[CrossRef](#)] [[PubMed](#)]
35. Jin, H.; Wang, J.; Su, D.; Wei, Z.; Pang, Z.; Wang, Y.; Am, J. In situ Cobalt-Cobalt Oxide/N-Doped Carbon Hybrids as Superior Bifunctional Electrocatalysts for Hydrogen and Oxygen Evolution. *Chem. Soc.* **2015**, *137*, 2688–2694. [[CrossRef](#)]

36. Zhang, B.; Zheng, X.; Voznyy, O.; Comin, R.; Bajdich, M.; Garcíamelchor, M.; Han, L.; Xu, J.; Liu, M.; Zheng, L. Homogeneously dispersed multimetal oxygen-evolving catalysts. *Sci. Found. China* **2016**, *352*, 51. [[CrossRef](#)]
37. Elisa, P.; Emanuele, L.; Sebastiano, B.; Danil, W.B.; Antonio, P.; Bekir, G.; Songül, D.; Mirko, P.; Silvia, G.; Reinier, O.N.; et al. Liquid-Phase Exfoliated Indium-Selenide Flakes and Their Application in Hydrogen Evolution Reaction. *Small* **2018**, *26*, 1800749.
38. Hu, Z.; Li, Q.; Lei, B.; Zhou, Q.; Xiang, D.; Lyu, Z.; Hu, F.; Wang, J.; Ren, Y.; Guo, R. Water-Catalyzed Oxidation of Few-Layer Black Phosphorous in a Dark Environment. *Angew. Chem. Int. Ed.* **2017**, *56*, 9131–9135. [[CrossRef](#)]
39. Kwak, I.H.; Im, H.S.; Dong, M.J.; Kim, Y.W.; Park, K.; Lim, Y.R.; Cha, E.H.; Park, J. CoSe<sub>2</sub> and NiSe<sub>2</sub> Nanocrystals as Superior Bifunctional Catalysts for Electrochemical and Photoelectrochemical Water Splitting. *ACS Appl. Mater. Interfaces* **2016**, *8*, 5327–5334. [[CrossRef](#)]

**Disclaimer/Publisher's Note:** The statements, opinions and data contained in all publications are solely those of the individual author(s) and contributor(s) and not of MDPI and/or the editor(s). MDPI and/or the editor(s) disclaim responsibility for any injury to people or property resulting from any ideas, methods, instructions or products referred to in the content.